4306–4314 *Nucleic Acids Research, 2017, Vol. 45, No. 8* *Published online 23 March 2017*
doi: 10.1093/nar/gkx202

Programmable i-motif DNA folding topology for a pH-switched reversible molecular sensing device

Lili Shi, Pai Peng, Yi Du and Tao Li*

Department of Chemistry, University of Science and Technology of China, 96 Jinzhai Road, Hefei, Anhui 230026, China

Received January 11, 2017; Revised March 02, 2017; Editorial Decision March 15, 2017; Accepted March 18, 2017

ABSTRACT

Four-stranded DNAs including G-quadruplexes and i-motifs are formed from four stretches of identical bases (G or C). A challenge remains in controlling the intermolecular folding of different G-rich or C-rich strands due to the self-association of each component. Here, we introduce a well-designed bimolecular i-motif that does not allow the dimerization of the same strand, and illustrate its usefulness in a pH-switched ATP-sensing DNA molecular device. We analyze two groups of i-motif DNAs containing two stretches of different C-residues ($C_{n-1}T_mC_n$ and $C_nT_mC_{n-1}$; $n = 3–6$, $m = 1, 3$) and show that their bimolecular folding patterns (L- and H-form) noticeably differs in the thermal stability. The L-form structures generally display a relatively low stability, with a bigger difference from that of conventional i-motifs formed by $C_nT_mC_n$. It inspires us to at utmost improving the structural stability by extending the core of L-form bimolecular i-motifs with a few flanking noncanonical base pairs, and therefore to avoid the dimeric association of each component. This meaningful bimolecular i-motif is then incorporated into a three-way junction (3WJ) and a four-way junction (4WJ) functionalized with two components of a ATP-binding split DNA aptamer, allowing the pH-triggered directional assembly of 3WJ and 4WJ into the desired (3+4)WJ structure that is verified by gel electrophoresis. It therefore enables the ATP-induced association of the split aptamer within the (3+4)WJ structure, as monitored by fluorescence quenching. In this way, the designed DNA system behaves as a pH-switched reversible molecular device, showing a high sensitivity and selectivity for fluorescent ATP analysis. The i-motif folding topology-programmed DNA nanoassembly may find more applications in the context of larger 2D/3D DNA nanostructures like lattices and polyhedra.

INTRODUCTION

DNA molecules have been extensively utilized as versatile construction materials to build varieties of mechanical nanodevices such as switches (1–5), walkers (6–9) and robots (10–12). In addition to Watson-Crick double-stranded structures, a large box of functional DNAs including aptamers (11,13,14), DNAzymes (10,15,16), triplexes (4,17), G-quadruplexes (18–21) and i-motifs (18,22–24) have been employed for DNA nanomechanics. G-quadruplexes and i-motifs are four-stranded DNA structures that share a common feature, namely that they are formed from four stretches of identical bases (G or C). Therefore, the intermolecular assembly among different G-rich or C-rich strands cannot be easily controlled due to their self-association. To solve this difficulty, some antiparallel or parallel double-stranded handles have been employed for guided assembly of intermolecular G-quadruplexes (25–27). Alternatively, different i-motif-functionalized DNA units can be put into an interlocked structure where the unwanted interstructural association of bimolecular i-motifs is prevented (18). Herein, we introduce a novel bimolecular i-motif that is exclusively designed to solve the difficulties in the uncontrollable self-association of intermolecular four-stranded DNAs.

Conventional C-rich DNAs with two C-tracts of the same length can adopt a head-to-head or head-to-tail folding pattern (Figure 1A, left panel) (24,28,29), influenced by the sequences of loops (28). Altering the length of C-tracts, these C-rich DNAs can also fold into tetramolecular (30), or even unimolecular i-motif structures (24). This polymorphism illustrates the difficulties to face when devising a desirable bimolecular i-motif structure. For this reason, some alterations in the sequences of bimolecular i-motif DNAs are required. For example, a C-rich DNA with two stretches of three and two C-residues has been reported to form an unusual bimolecular i-motif structure consisting of five $C{\bullet}C^+$ base pairs (iM5), namely, the length of two parallel $C{\bullet}C^+$ base-paired duplexes is different (Figure 1A, middle panel) (31). This kind of i-motif DNAs in principle only favors the head-to-head folding pattern, with an extra outside $C{\bullet}C^+$ base pair at the 5′ or 3′ terminus (henceforth designated H-

*To whom correspondence should be addressed. Tel: +86 551 63601813; Fax: +86 551 63601813; Email: tlitao@ustc.edu.cn

© The Author(s) 2017. Published by Oxford University Press on behalf of Nucleic Acids Research.
This is an Open Access article distributed under the terms of the Creative Commons Attribution License (http://creativecommons.org/licenses/by-nc/4.0/), which permits non-commercial re-use, distribution, and reproduction in any medium, provided the original work is properly cited. For commercial re-use, please contact journals.permissions@oup.com

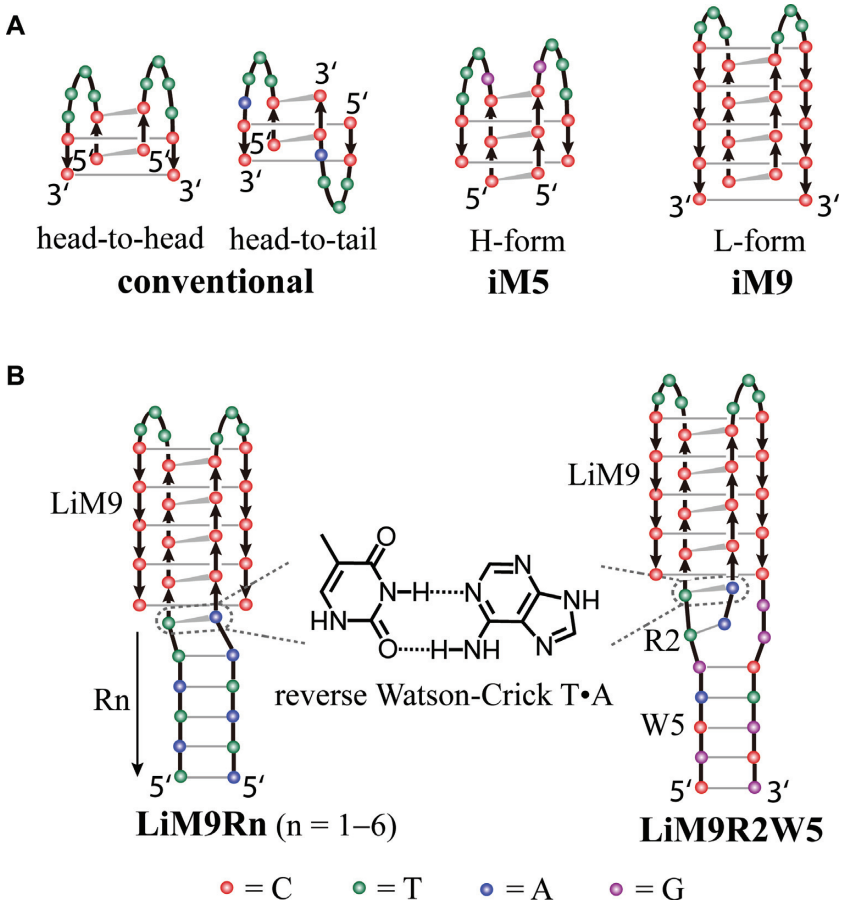

Figure 1. Structural design of bimolecular i-motifs. (**A**) Left: Two possible folding patterns of conventional bimolecular i-motif DNAs. The head-to-head and head-to-tail structures are found in the bimolecular i-motifs formed by *d*(5-methyl-CCTTTTCC) and *d*(5-methyl-CCTTTACC), respectively (28). Middle: An H-form bimolecular i-motif structure formed by $C_3GT_3C_2$ consisting of five C•C$^+$ base pairs (iM5), with the extra pair at 5′ terminus (31). Right: Favorable L-form structure of a bimolecular i-motif formed by $C_4T_3C_5$ consisting of nine C•C$^+$ base pairs (iM9), with the extra pair at 3′ terminus. Here, the H- and L-form are named from a high or low stability of unusual i-motif structures containing the same C•C$^+$ base pairs. (**B**) i-motif design by extending the core of LiM9 with flanking a reverse Watson–Crick T•A base pair (in dash circle). A few noncanonical base pairs (left) or a Watson–Crick double-stranded motif (right) is introduced to further stabilize the structure of this bimolecular i-motif. The designed i-motif LiM9R2W5 in the right panel proves a desirable structure in this study.

or L-form). In addition to the C•C$^+$ pairs, flanking a few noncanonical base pairs can also be employed to extend the core of i-motif structures (32,33), contributed to a higher stability. Therefore, a systematic understanding of not only the folding of unusual i-motif DNAs but also the influence of flanking base pairs will be useful for designing new DNA topologies.

Herein, we systematically study the folding of two groups of unusual i-motif DNAs, $C_{n\text{-}1}T_mC_n$ and $C_nT_mC_{n\text{-}1}$, by polyacrylamide gel electrophoresis (PAGE), circular dichroism (CD) and thermal denaturation. We find that these two groups of bimolecular i-motifs noticeably differ in the thermal stability. The L-form structures folded from $C_{n\text{-}1}T_mC_n$ (e.g. $C_4T_3C_5$) generally display a relatively low stability (Figure 1A, right panel). With a few flanking noncanonical base pairs, we devise and improve L-form bimolecular i-motifs (Figure 1B, right panel), and employ them to direct the pH-triggered assembly of two DNA branched junctions into a desired nanoarchitecture where reversible ATP capture and sensing are accomplished, verified by gel electrophoresis and fluorescence quenching.

MATERIALS AND METHODS

i-motif DNAs

PAGE-purified and MS-verified C-rich DNAs were obtained from Sangon Biotechnology (Shanghai, China) and quantified by using an Agilent cary60 UV–vis spectrometer (Santa Clara, USA). Each DNA (10 μM) was incubated at 90°C for 5 min in the TAE buffer (40 mM Tris–Ac buffer, 0.1 mM EDTA, pH 5) containing 2 mM $MgCl_2$, then slowly cooled and incubated at 4°C overnight, allowing C-rich DNAs to properly fold into the i-motif structures.

Native PAGE

Non-denaturing polyacrylamide gel (18%) was used for i-motif DNAs and prepared in the TAE buffer (pH 5) containing 2 mM $MgCl_2$. Gel electrophoresis was run in the same buffer at 4°C for 6 h under a voltage of 8 V/cm. The gel was then stained in 0.01% Stains-All solution and destained under light, finally photographed with a camera.

9% non-denaturing polyacrylamide gel was used for DNA nanostructures and run under 10 V/cm for 9 h. The gel was then stained by GelRed, photographed under UV light with Tanon 1600 Gel Imaging System (Shanghai, China).

CD measurements

The CD spectra of 50 μM C-rich DNAs at pH 5 in the TAE buffer containing 2 mM $MgCl_2$ were collected at 4°C with a JASCO J-1500 spectropolarimeter (Tokyo, Japan) equipped with a Peltier temperature controller. The optical chamber (1-mm path length, 400 μl) was deoxygenated with dry purified nitrogen before use and kept the nitrogen atmosphere during experiments. Three scans from 220 to 330 nm were accumulated and averaged. In each case, the background of the buffer solution was subtracted from the CD data.

Melting curves

The melting curves of 50 μM DNA i-motifs at pH 5 in the TAE buffer containing 2 mM $MgCl_2$ were monitored at 290 nm by the J-1500 spectropolarimeter, with a rate of 0.5°C/min. The CD signal at 290 nm (CD_{290}) was normalized in each case. The T_m value of i-motifs was obtained at which 50% of i-motif structures were dissociated.

DNA molecular device

The designed DNA system consists of a three-way junction (3WJ) and a four-way junction (4WJ). The two components of both i-motif DNA and ATP-binding split aptamer are tethered to the ends of two arms of 3WJ and 4WJ, respectively. 300 nM of 3WJ and 4WJ structures were separately prepared, mixed at equivalent molar concentration, then incubated at 37°C for 4 h in the TAE buffer (pH 5) containing 5mM $MgCl_2$ and 300 mM NaCl, followed by incubating with different concentrations of ATP for 1 h. This allows the formation of the i-motif structure that promotes the split aptamer to bind ATP, indicated by gel electrophoresis and fluorescence quenching.

Fluorescence spectroscopy

The fluorescently labeled 3WJ and 4WJ were operated in the TAE buffer (pH 5) containing 5 mM $MgCl_2$ and 300 mM NaCl at a working concentration of 200 nM. The pH value of this DNA system was switched between pH 5 and 8 by alternate addition of 0.4% (v/v) 6 M HCl and 6 M NaOH. After each pH switch, the system was incubated at 60°C for 30 min, allowing the i-motif DNA on the end of two branched junctions to properly fold. Subsequently, the sample was cooled slowly to room temperature for fluorimetry. The fluorescence spectra were recorded by a Hitachi F-4600 Fluorescence spectrometer (Tokyo, Japan) with an excitation wavelength at 550 nm. For each measurement, a control system without ATP was used and monitored in parallel to normalize the fluorescence signal.

RESULTS

Unusual bimolecular i-motif DNAs and structural design

Compared to conventional bimolecular i-motif DNAs that possibly fold in the head-to-head or head-to-tail pattern (Figure 1A, left panel) (24,28,29), the head-to-head structures formed by unusual i-motif DNAs (31) are more easy to be predicted and employed for the i-motif design. Therefore, here we primarily tested two groups of unusual i-motif DNAs, $C_{n\text{-}1}T_mC_n$ and $C_nT_mC_{n\text{-}1}$ ($n = 3-6$, $m = 1, 3$), and aimed at identifying robust bimolecular four-stranded structures suitable for being employed as construction components in large DNA nanoarchitectures. As two stretches of over six C-residues favor the intramolecular folding of i-motifs (24), the length of C-tracts in tested DNAs ranges from two to six, while the length of all sequences is kept approximate via altering the number of T-residues on the two ends (see Supplementary Table S1).

We employed native PAGE to analyze the structures formed by these C-rich DNAs at pH 5, together with $C_{n\text{-}1}T_mC_{n\text{-}1}$ and a single-stranded random sequence $(TCT)_4$. A faster moving single band appears for $C_2T_3C_2$, $C_2T_3C_3$ and $C_3T_3C_2$, consistent with the single strand (Figure 2A, lanes 1–4). It indicates that these DNAs are unfolded under electrophoretic conditions employed here, confirmed by CD spectroscopy (Figure 2B). These DNAs mainly have a positive peak around 280 nm in the CD spectra, consistent with that of C-rich single strands (34). The same phenomena are observed when shortening their linkers (see Figure S1A and B in Supporting Information). These unfolded DNAs were no longer tested below.

When the n value varies from 4 to 6, the bands of tested DNAs have a lower mobility (Figure 2A, lanes 5–13), although their sequence length is approximate to that of $C_2T_3C_2$, $C_2T_3C_3$ and $C_3T_3C_2$. This is attributed to the formation of bimolecular i-motif structures (24), verified by thermal denaturation that shows a concentration dependence of their structural stability (see Figure S2 in Supporting Information). CD spectroscopy was also utilized to confirm the formation of i-motif structures (Figure 2B). All of these C-rich DNAs display a dominant positive band around 290 nm and a negative one near 265 nm in the corresponding CD spectra, consistent with the characteristics of i-motif structures (35). In some case, however, the polymorphism of i-motif folding is observed (Figure 2A, lanes 8–13). Both $C_4T_3C_4$ and $C_5T_3C_5$ (lanes 8 and 11) have a broad band, implying the formation of more than one conformations. In fact, this kind of bimoleucalr i-motifs are prone to form two or more isomers that are sometimes observed in gel electrophoresis (36,37). For $C_4T_3C_5$ and $C_5T_3C_4$ (lanes 9–10), especially for $C_5T_3C_6$ and $C_6T_3C_5$ (lanes 12–13), a dominant band is followed by a faint tail, possibly owing to their diffusion during gel electrophoresis. In contrast, those i-motif DNAs with shorter linkers do not so (see Figure S1A in Supporting Information).

Figure 2C shows that the thermal stability of these i-motif DNAs is enhanced as the length of C-tracts increases (i.e. $n = 4 \rightarrow 6$), and that is true when shortening the linkers (see Figure S1C in Supporting Information). It is conceivable that longer C-tracts allow the formation of more $C{\bullet}C^+$ base

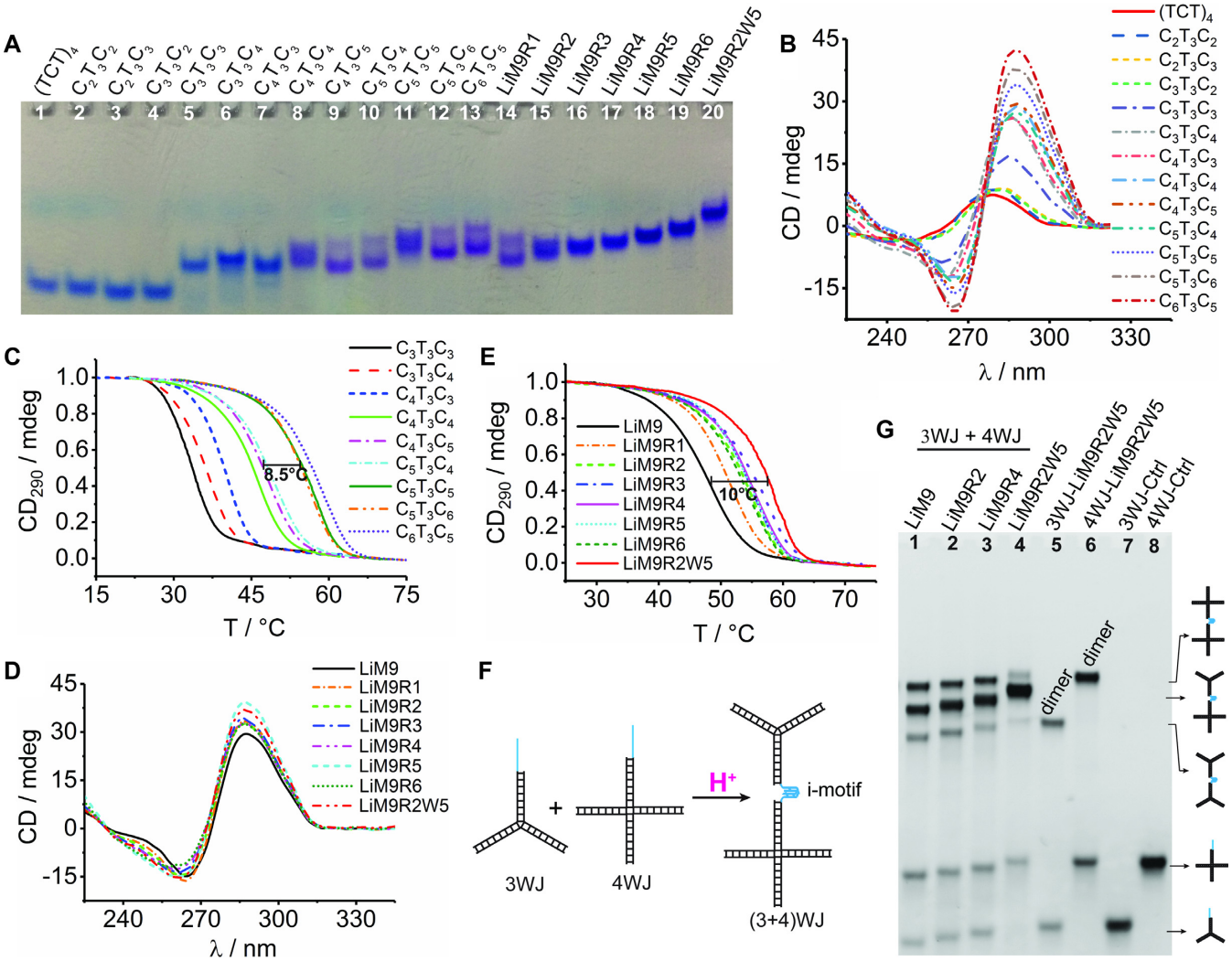

Figure 2. Investigations of bimolecular i-motif DNAs. (**A**) Electrophoretograms of 200 pmol DNAs in 18% native polyacrylamide gels under acidic conditions. In lanes 1–4, only one faster moving band exists, indicating no secondary structure formed under the conditions employed here. In lanes 5–20, the bands with slower mobility correspond to the bimolecular i-motifs, and the polymorphism is observed in lanes 8–14. (**B**) CD spectra of C-rich DNAs (50 μM) under acidic conditions. In each case, the CD spectral characteristics of a dominant positive band around 290 nm and a negative one near 265 nm shows the formation of corresponding i-motif structures. (**C**) Melting curves that are corresponding to B). (**D**) CD spectra of devised bimolecular i-motif DNAs (50 μM) under acidic conditions. (**E**) CD melting curves of i-motif DNAs (50 μM) monitored at 290 nm. (**F**) Schematic for the programmable assembly of i-motif-functionalized DNA branched junctions (3WJ and 4WJ) into the desired (3+4)WJ nanoarchitecture under acidic conditions. (**G**) Electrophoretograms of different i-motif-conjugated nanostructures (3 pmol) in 9% native polyacrylamide gels under acidic conditions. In lane 4, a dominant band corresponding to the (3+4)WJ nanoarchitecture is observed, whereas a large amount of unwanted dimers of both 3WJ and 4WJ always coexist in lanes 1–3.

pairs to participate in the core of i-motif structures, contributing to an increase in the stability (24). Interestingly, we always observed a noticeable difference between the thermal stability of $C_{n\text{-}1}T_mC_n$ and $C_nT_mC_{n\text{-}1}$, regardless of the length of linkers, suggesting that they fold into two distinct i-motif structures. The folded structures of $C_nT_mC_{n\text{-}1}$ always have a higher stability, and favor the H-form folding pattern resembling that of $C_3GT_3C_2$ determined by NMR (31) (Figure 1A, middle panel). It's conceivable that certain a C residue of $C_nT_mC_{n\text{-}1}$ may be not engaged in the core structure but is part of one loop of the resulting i-motifs (see Figure S3A in Supporting Information). In terms of thermal stability, however, this possibility can be rationally excluded (Supplementary Figure S3B). Likewise, the L-form pattern is most favorable for the folding of $C_{n\text{-}1}T_mC_n$ that displays a relatively low stability (Figure 1A, right panel), with a bigger difference between that of folded $C_nT_mC_n$ (Table 1). For example, the melting temperature (T_m) of $C_4T_3C_5$ is 8.5°C lower than that of $C_5T_3C_5$. These observations inspire us to at utmost improving the structural stability via extending the core of L-form i-motifs with flanking noncanonical base pairs (Figure 1B).

Since the i-motif core structure consists of two parallel C•C^+ base-paired duplexes, we primarily tested a few reverse Watson-Crick T•A base pairs that can stabilize parallel duplexes (27). A NMR study has demonstrated that an analogue U•A base pair is able to participate in and therefore extend the core of an intramolecular i-motif structure

Table 1. Melting temperatures of the i-motif structures tested in Figure 1A, except for those unfolded DNAs

Name	T_m (°C)	Name	T_m (°C)
$C_3T_3C_3$	33.4	$C_6T_3C_5$	59.1
$C_3T_3C_4$	37.1	LiM9R1	53.0
$C_4T_3C_3$	40.1	LiM9R2	55.0
$C_4T_3C_4$	46.2	LiM9R3	55.3
$C_4T_3C_5$	48.8	LiM9R4	55.4
$C_5T_3C_4$	49.9	LiM9R5	55.2
$C_5T_3C_5$	57.3	LiM9R6	54.2
$C_5T_3C_6$	57.8	LiM9R2W5	58.8

(32). Likewise, we sought to extend the i-motif core structure of LiM9 with a flanking reverse Watson-Crick T•A base pair, followed by up to five ones to further stabilize the structure (Figure 1B, left panel). Another approach to extending the i-motif core structures is also tested, and it does not improve but rather decreases the thermal stability (see Figure S4 in Supporting Information). PAGE shows that these devised i-motif DNAs all fold into bimolecular i-motifs (Figure 2A, lanes 14−19), evidenced by CD spectroscopy (Figure 2D). The thermal stability of i-motif structure is remarkably enhanced by at most four noncanonical T•A base pairs, especially within two ones (Figure 2E).

When incorporated into the single-stranded terminus of DNA branched junctions (Figure 2F), however, the candidate i-motifs LiM9R2 and LiM9R4 cannot direct most of branched junctions to assemble into the desired (3+4)WJ nanoarchitecture, as the dimers of 3WJ and 4WJ do not disappear in spite of an observable improvement (Figure 2G, lanes 2, 3; versus lane 1). Therefore, we sought to solve this problem by introducing a Watson-Crick double-stranded motif that follows two noncanonical T•A base pairs (Figure 1B, right panel). The resulting i-motif DNA named LiM9R2W5 also folds into a bimolecular structure, verified by PAGE (Figure 2A, lane 20) and CD spectroscopy (Figure 2D). Thermal denaturation shows that LiM9R2W5 displays a far higher stability (ΔT_m = 10°C) than the unimproved counterpart LiM9 (Figure 2E). Consequently, LiM9R2W5-functionalized DNA branched junctions are prone to a programmable assembly into the (3+4)WJ nanoarchitecture responding to pH change, while the LiM9-conjugated dimers of both 3WJ and 4WJ are almost prevented due to much lower robustness compared to the LiM9R2W5-mediated conjugation (Figure 2G, lane 4−6). This highlights a unique advantage of the devised bimolecular i-motif DNA over other counterparts employed previously (18,24).

Under the conditions employed here, LiM9R2W5 exhibits a high thermal stability (T_m = 58.8°C) approximating to that of the most stable bimolecular i-motif (C_6TC_6) known to date (24). Due to the structural robustness and controllable folding, this well-designed i-motif DNA can serve as a useful construction component to build nanomechanical devices (Table 1).

pH-switched ATP-sensing DNA molecular device

Based on the insight into the folding of bimolecular i-motif DNAs, we next sought to employ them for the controllable assembly of two DNA branched nanostructures, a three-way junction (3WJ) and a four-way junction (4WJ), to build a pH-switched reversible molecular device for ATP capturing and sensing (Figure 3A). Two single-stranded motifs are tethered to their two adjacent arms, that can be functionalized at will with different DNA sequences (38). Thereby, the functionalized branched junctions can serve as versatile construction components that can be incorporated, for example, into larger 2D/3D DNA nanoarchitectures such as lattices (39,40) and polyhedra (41,42).

Here, LiM9R2W5 and an ATP-binding split DNA aptamer (43) are employed to functionalize the two single-stranded motifs of 3WJ and 4WJ (Figure 3A, left panel), resulting in two working structures named 3WJ-C4-ABA and 4WJ-C4-ABA. The folding of the bimolecular i-motif allows the working structures to respond to pH change and accomplish the assembly into a desired larger (3+4)WJ nanoarchitecture (Figure 3A, middle panel), a scaffold for the ATP-induced intrastructural association of the split aptamer (Figure 3A, right panel).

We analyzed the electrophoretic behaviors of 3WJ-C4-ABA and 4WJ-C4-ABA assembled in different states by native PAGE (Figure 3B−D). Under acidic conditions, one dominant band with slow electrophoretic mobility was observed (Figure 3B, lane 1), corresponding to the (3+4)WJ nanoarchitecture that moves slightly faster than an i-motif-conjugated reference structure (lane 2) in which two components of the split aptamer are replaced by random sequences. Upon addition of ATP, there is a slight decrease in the electrophoretic mobility of the (3+4)WJ nanoarchitecture as compared with the reference structure (Figure 3C, lane 1 versus lane 2). It reveals that the ATP−aptamer interaction lowers the mobility of the (3+4)WJ nanoarchitecture possibly due to a size increase, and a similar phenomenon has been reported previously (5). Upon adjusting the pH to 8, the above slowest bands disappears and meanwhile those of two branched junctions become clearer (Figure 3D, lanes 1 and 2), indicating a disruption of the (3+4)WJ nanoarchitecture. We noticed that the band corresponding to an ATP aptamer-conjugated (3+4)WJ structure does not appear in each case (Figure 3B−D, lane 3), indicating no uncontrollable association of the working structures induced by ATP alone. These observations demonstrate that the ATP binding by the split aptamer tethered to the DNA nanostructures highly depends on the formation of the bimolecular i-motif structure under acidic conditions, illustrating a rationale for the construction of a pH-switched ATP-captured DNA molecular device based on the i-motif-controlled DNA nanoassembly.

To further demonstrate the ATP-induced association of the split aptamer in the i-motif-conjugated architecture, we performed a fluorescence quenching (FQ) study by labeling two components of the aptamer with carboxytetramethylrhodamine (TAMRA) and a quencher (BHQ2). This results

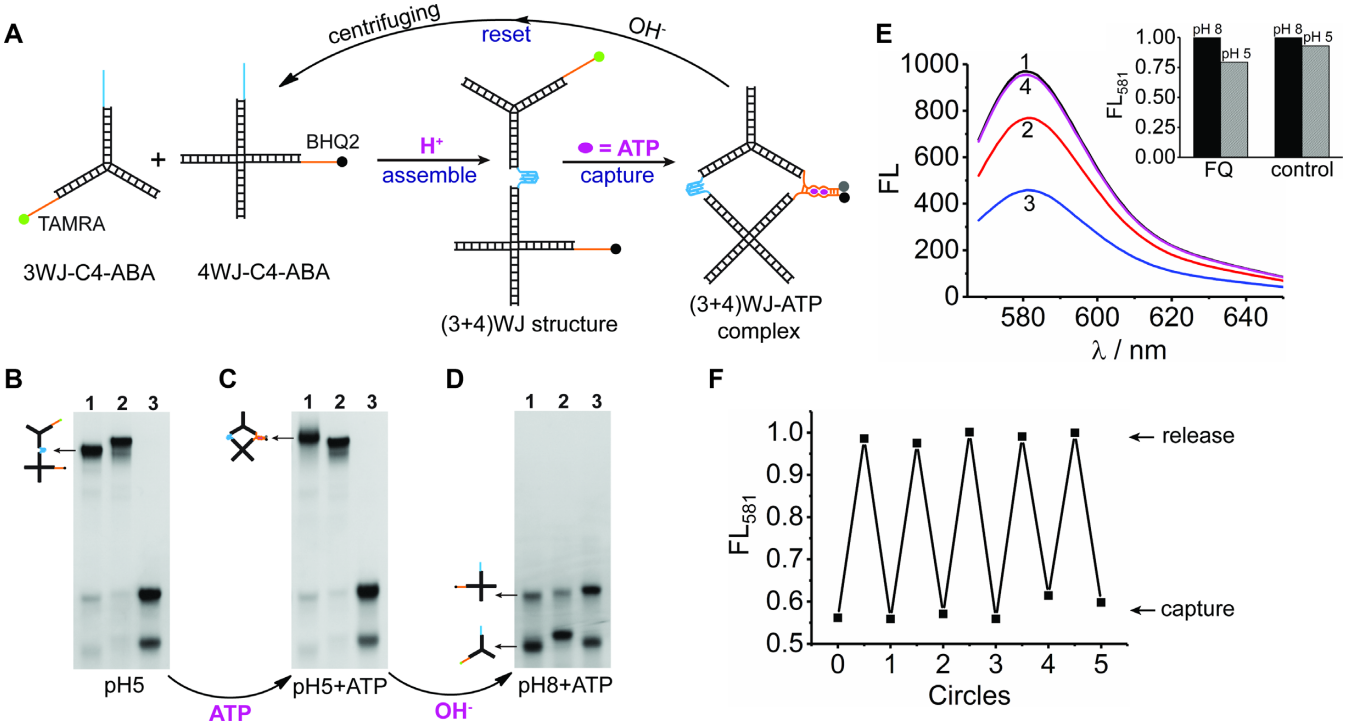

Figure 3. A pH-switched DNA molecular device for the reversible capture and release of ATP molecules. (**A**) Schematic for the working principle of a fluorescence quenching (FQ) system built on the assembly/disassembly of DNA branched junctions in response to pH change. The designed primary structures 3WJ-C4-ABA and 4WJ-C4-ABA both have two single-stranded termini on their two arms that are functionalized with two components of the bimolecular i-motif LiM9R2W5 (cyan) and the fluorescently labeled ATP-binding split DNA aptamer (orange). The folding of i-motif DNA enables the branched structures to respond to pH change and accomplish the association between 3WJ and 4WJ, therefore allowing the intrastructural association of two components of the split aptamer upon addition of ATP. (**B**) Electrophoretograms of the assembled nanostructures (3 pmol) in 9% native polyacrylamide gels under acidic conditions. Lane 1: the working system consisting of 3WJ-C4-ABA and 4WJ-C4-ABA; Lane 2: reference structures 3WJ-C4 and 4WJ-C4 resulting from replacing the split aptamer by random sequences; Lane 3: reference structures 3WJ-ABA and 4WJ-ABA resulting from replacing the i-motif DNA by random sequences. (**C**) Electrophoretograms of DNA nanostructures in panel (B) upon addition of 200 μM ATP. An observable shift in the electrophoretic mobility of the (3+4)WJ nanoarchitecture originates from two ATP molecules captured by the split aptamer (lane 1 versus lane 2, compared to panel B), consistent with previous observations (5). (**D**) Electrophoretograms of DNA nanostructures in panel C upon adjusting pH to 8. In the presence of ATP alone, the band corresponding to an ATP-conjugated (3+4)WJ structure was not observed in lane 3 (panels C and D), indicating that the unwanted interstructural association of two components of this split aptamer does not occur in each case. (**E**) Fluorescence spectra of the FQ system in different states: 1, as-prepared at pH 8; 2, adjusting pH of the state 1 to 5; 3, adding 200 μM ATP into the state 2; 4, adjusting pH of the state 3–8. Upon addition of ATP, a sharp decrease in the fluorescence intensity was observed at pH 5, indicating that the dye and quencher are close and therefore fluorescence quenching occurs in this case. The insert shows an obvious proton-induced fluorescence decrease in the FQ system whereas the control structures 3WJ-ABA and 4WJ-ABA do not so, suggesting that a slight fluorescence quenching occurs between TAMRA and BHQ2 in the i-motif-conjugated (3+4)WJ nanoarchitectrue. (**F**) Working cycles of the ATP-captured DNA molecular device switched between pH 5 and 8 in the presence of 500 μM ATP, indicating the reversible capture and release of ATP molecules by a decrease and increase in the fluorescence intensity at 581 nm (FL_{581}). The fluorescence intensity was normalized in each case.

in a reversible FQ system in which the pH-controlled capture and release of ATP molecules can be monitored (Figure 3A). As a control, the reference system resulting from the i-motif DNA replaced by random sequences was labeled in the same way and monitored in parallel. TAMRA displays a pH-insensitive fluorescence emission so that it can work in a wide pH range (24). At pH 8, the i-motif DNA is unfolded and the two branched junctions are separate, namely, the dye and quencher are separate and no FQ occurs. Indeed, a bright fluorescence is observed in this case (Figure 3E, curve 1). When adjusting the pH to 5, there is a ca. 21% decrease in the fluorescence intensity (Figure 3E, curve 2). In contrast, the reference system only shows a small (∼7%) fluorescence decrease (Figure 3E, insert) that is mainly due to a slightly lower efficiency of TAMRA fluorescence emission under acidic conditions (24). This comparison suggests that FQ occurs slightly between TAMRA and BHQ2 in the i-motif-conjugated nanoarchitecture, as they are a little closer than in the separated two branched junctions. Following pH adjusting, the addition of ATP gives rise to a sharp decrease in the fluorescence intensity (Figure 3E, curve 3), attributed to the ATP-induced association of the split aptamer that holds TAMRA and BHQ2 closely (illustrated in Figure 3A, right panel). The FQ system can be reset by adjusting pH to 8 to disrupt the i-motif structure and therefore to release the bound ATP, reflected by an increase in the fluorescence intensity (Figure 3E, curve 4). By switching pH between 5 and 8, the system can be further operated many times in a fully reversible fashion (Figure 3F) (22,24,44–48). In this way, the working system behaves as a DNA molecular device that can be switched back and forth between the association and disassembly states, and reversibly captures and releases ATP molecules.

From the view of ATP analysis, the above-described

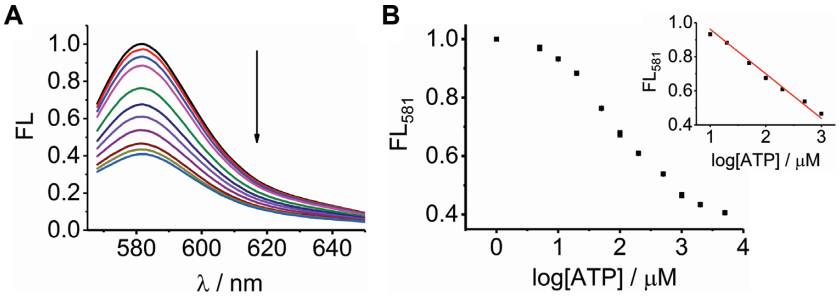

Figure 4. pH-switched DNA molecular device as a reversible ATP nanosensor. (**A**) Fluorescence spectra of the FQ system responding to different concentrations of ATP (from top to bottom): 0, 5, 10, 20, 50, 100, 200, 500, 1000, 2000, 5000 μM. (**B**) Plot of the fluorescence intensity at 581 nm (FL_{581}) versus the logarithm of ATP concentration (log[ATP]). The insert shows a good linear relationship in the range from 10 to 1000 μM. The fluorescence intensity was normalized in each case.

DNA molecular device indeed behaves as a conceptually new reversible ATP nanosensor with a pH switch. To test the ability to probing ATP by such a nanosensor, the fluorescence spectra of TAMRA were recorded by varying the concentration of ATP under acidic conditions (Figure 4A). As the concentration of ATP increases, the fluorescence intensity decreases gradually. The plot of the fluorescence intensity at 581 nm (FL_{581}) versus the logarithm of ATP concentration (log[ATP]) shows that 5 μM ATP can induce a noticeable change in the fluorescence intensity (Figure 4B), revealing a limit of detection (5 μM) for ATP analysis with a linear relationship ($R^2 = 0.993$) in range of 10−1000 μM (Figure 4B, insert). However, If LiM9R2W5 in the DNA nanostructures is replaced by the previously used bimolecular i-motif C_6TC_6 (18,24), an observable decrease in the fluorescence intensity is only observed in the presence of over 100 μM ATP (see Figure S6 in Supporting Information), indicating a poor sensitivity 20 times lower than that of the present study. This highlights an advantage of our designed i-motif over previous counterparts. Furthermore, the selectivity for ATP analysis was tested by using other analogues including CTP, GTP and UTP in place of ATP (see Figure S7 in Supporting Information). It shows that only ATP causes a remarkable decrease in fluorescence signal, indicating a high selectivity of this nanosensor for ATP detection that is comparable with those of previously reported fluorescent ATP aptasensors (49,50). By adjusting pH to 8 and then removing ATP with centrifugal filter devices (5), the reuse of this nanosensor would be achieved. This is a main difference of our study compared to most of previous reports (49,50).

DISCUSSION

We have systematically studied the bimolecular folding of two groups of i-motif DNAs with two stretches of different C-residues by PAGE, CD and thermal denaturation, revealing a noticeable difference in the thermal stability of two possible folding patterns of these unusual bimolecular i-motifs. The L-form i-motifs such as $C_3T_3C_4$ and $C_4T_3C_5$ generally display a relatively low stability as compared to $C_4T_3C_3$ and $C_5T_3C_4$ that fold into H-form i-motifs (Figure 2). Based on the L-form structure of $C_4T_3C_5$, we have devised a remarkably improved bimolecular i-motif named LiM9R2W5 with an extended core by flanking two non-canonical base pairs (32) and then a Watson-Crick double-stranded motif. Such a meaningful i-motif structure shows a unique feature that the dimerization of its two components is prevented, in contrast to other counterparts (24,28,29). This allows it to be employed for the controllable assembly of 3WJ and 4WJ functionalized with the two components of the ATP-binding split DNA aptamer (43). The system responds to pH change, and forms the i-motif-conjugated (3+4)WJ nanoarchitecture that favors the ATP-induced intrastructural association of the split aptamer whereas the unwanted interstructural interaction rarely occurs (Figure 3). In this way, the system has been repeatedly operated as a pH-switched DNA molecular device controlling the reversible capture and release of ATP. When used for ATP analysis, such a DNA molecular device exhibits a high sensitivity and selectivity (Figure 4), illustrating a new concept for the design and construction of reversible nanosensors (5).

Note that the 'core' concept for devising this ATP-sensing DNA molecular device is controlling the intrastructural association of the split aptamer by the pH-dependent folding of bimolecular i-motif DNAs. Some undesired ATP-induced interstructural interactions may occur between 3WJ-C4-ABA and 4WJ-C4-ABA (Figure 3A, left panel) or two molecules of (3+4)WJ nanoarchitecture (Figure 3A, middle panel), highly depending on the concentrations of the DNA structures (24). Under the conditions employed here, the ATP-induced unwanted structures rarely form, as indicated in Figure 3C and D. At higher concentrations, however, a faint band of the ATP-confugated (3+4)WJ structure appears in gel electrophoretograms (data not shown). These observations suggest that at lower ATP concentrations the ATP-aptamer hybrid complex is not robust enough to stably connect the large-size DNA structures 3WJ and 4WJ. This concentration-dependent feature may become useful in the context of bimolecular i-motif-functionalized 2D/3D DNA nanostructures like lattices (39,40) and polyhedra (41,42), of which the undesired interstructural interactions between two or more molecules of lattices or polyhedra would be avoided by DNA concentration control.

Our study provides insight into the controllable folding of bimolecular i-motif DNAs (24,28,29,31), and demonstrates how to harness this knowledge for the controllable assembly of DNA branched nanostructures. It will open new ways to

operate larger DNA nanoarchitectures like lattices (39,40) and polyhedra (41,42) to achieve varieties of mechanical operation. For example, the components of different bimolecular i-motifs may be tethered to different edges of a tetrahedron to open and close different faces, which may find further applications in pH-controlled loading and release of cargos when using a tetrahedron as a carrier.

SUPPLEMENTARY DATA

Supplementary Data are available at NAR Online.

FUNDING

National Natural Science Foundation of China [21575133]; National Key Research and Development Program of China [2016YFA0201300]; Recruitment Program of Global Experts. Funding for open access charge: Recruitment Program of Global Experts.
Conflict of interest statement. None declared.

REFERENCES

1. Lohmann,F., Ackermann,D. and Famulok,M. (2012) Reversible light switch for macrocycle mobility in a DNA rotaxane. *J. Am. Chem. Soc.*, **134**, 11884–11887.
2. Ackermann,D. and Famulok,M. (2013) Pseudo-complementary PNA actuators as reversible switches in dynamic DNA nanotechnology. *Nucleic Acids Res.*, **41**, 4729–4739.
3. Lu,C.H., Qi,X.J., Cecconello,A., Jester,S.S., Famulok,M. and Willner,I. (2014) Switchable reconfiguration of an interlocked DNA olympiadane nanostructure. *Angew. Chem., Int. Ed.*, **53**, 7499–7503.
4. Idili,A., Vallee-Belisle,A. and Ricci,F. (2014) Programmable pH-triggered DNA nanoswitches. *J. Am. Chem. Soc.*, **136**, 5836–5839.
5. Peng,P., Shi,L., Wang,H. and Li,T. (2017) A DNA nanoswitch-controlled reversible nanosensor. *Nucleic Acids Res.*, **45**, 541–546.
6. Yin,P., Yan,H., Daniell,X.G., Turberfield,A.J. and Reif,J.H. (2004) A unidirectional DNA walker that moves autonomously along a track. *Angew. Chem., Int. Ed.*, **43**, 4906–4911.
7. Omabegho,T., Sha,R. and Seeman,N.C. (2009) A bipedal DNA Brownian motor with coordinated legs. *Science*, **324**, 67–71.
8. Wang,Z.G., Elbaz,J. and Willner,I. (2011) DNA machines: bipedal walker and stepper. *Nano Lett.*, **11**, 304–309.
9. Huang,F., You,M., Han,D., Xiong,X., Liang,H. and Tan,W. (2013) DNA branch migration reactions through photocontrollable toehold formation. *J. Am. Chem. Soc.*, **135**, 7967–7973.
10. Lund,K., Manzo,A.J., Dabby,N., Michelotti,N., Johnson-Buck,A., Nangreave,J., Taylor,S., Pei,R.J., Stojanovic,M.N., Walter,N.G. *et al.* (2010) Molecular robots guided by prescriptive landscapes. *Nature*, **465**, 206–210.
11. Douglas,S.M., Bachelet,I. and Church,G.M. (2012) A logic-gated nanorobot for targeted transport of molecular payloads. *Science*, **335**, 831–834.
12. Amir,Y., Ben-Ishay,E., Levner,D., Ittah,S., Abu-Horowitz,A. and Bachelet,I. (2014) Universal computing by DNA origami robots in a living animal. *Nat. Nanotechnol.*, **9**, 353–357.
13. Dittmer,W.U., Reuter,A. and Simmel,F.C. (2004) A DNA-based machine that can cyclically bind and release thrombin. *Angew. Chem., Int. Ed.*, **43**, 3550–3553.
14. Chhabra,R., Sharma,J., Ke,Y., Liu,Y., Rinker,S., Lindsay,S. and Yan,H. (2007) Spatially addressable multiprotein nanoarrays templated by aptamer-tagged DNA nanoarchitectures. *J. Am. Chem. Soc.*, **129**, 10304–10305.
15. Willner,I., Shlyahovsky,B., Zayats,M. and Willner,B. (2008) DNAzymes for sensing, nanobiotechnology and logic gate applications. *Chem. Soc. Rev.*, **37**, 1153–1165.
16. Elbaz,J., Lioubashevski,O., Wang,F., Remacle,F., Levine,R.D. and Willner,I. (2010) DNA computing circuits using libraries of DNAzyme subunits. *Nat. Nanotechnol.*, **5**, 417–422.
17. Wu,N. and Willner,I. (2016) pH-stimulated reconfiguration and structural isomerization of origami dimer and trimer systems. *Nano Lett.*, **16**, 6650–6655.
18. Li,T., Lohmann,F. and Famulok,M. (2014) Interlocked DNA nanostructures controlled by a reversible logic circuit. *Nat. Commun.*, **5**, 4940.
19. Sannohe,Y., Endo,M., Katsuda,Y., Hidaka,K. and Sugiyama,H. (2010) Visualization of dynamic conformational switching of the G-quadruplex in a DNA nanostructure. *J. Am. Chem. Soc.*, **132**, 16311–16313.
20. Alberti,P. and Mergny,J.L. (2003) DNA duplex-quadruplex exchange as the basis for a nanomolecular machine. *Proc. Natl. Acad. Sci. U.S.A.*, **100**, 1569–1573.
21. Alberti,P., Bourdoncle,A., Sacca,B., Lacroix,L. and Mergny,J.L. (2006) DNA nanomachines and nanostructures involving quadruplexes. *Org. Biomol. Chem.*, **4**, 3383–3391.
22. Liu,D. and Balasubramanian,S. (2003) A proton-fuelled DNA nanomachine. *Angew. Chem., Int. Ed.*, **42**, 5734–5736.
23. Wang,C., Huang,Z., Lin,Y., Ren,J. and Qu,X. (2010) Artificial DNA nano-spring powered by protons. *Adv. Mater.*, **22**, 2792–2798.
24. Li,T. and Famulok,M. (2013) I-Motif-Programmed Functionalization of DNA Nanocircles. *J. Am. Chem. Soc.*, **135**, 1593–1599.
25. Dutta,K., Fujimoto,T., Inoue,M., Miyoshi,D. and Sugimoto,N. (2010) Development of new functional nanostructures consisting of both DNA duplex and quadruplex. *Chem. Commun.*, **46**, 7772–7774.
26. Zhou,J., Bourdoncle,A., Rosu,F., Gabelica,V. and Mergny,J.L. (2012) Tri-G-quadruplex: controlled assembly of a G-quadruplex structure from three G-rich strands. *Angew. Chem., Int. Ed.*, **51**, 11002–11005.
27. Yatsunyk,L.A., Pietrement,O., Albrecht,D., Tran,P.L., Renciuk,D., Sugiyama,H., Arbona,J.M., Aime,J.P. and Mergny,J.L. (2013) Guided assembly of tetramolecular G-quadruplexes. *ACS Nano*, **7**, 5701–5710.
28. Nonin,S., Phan,A.T. and Leroy,J.L. (1997) Solution structure and base pair opening kinetics of the i-motif dimer of d(5mCCTTTACC): a noncanonical structure with possible roles in chromosome stability. *Structure*, **5**, 1231–1246.
29. Canalia,M. and Leroy,J.L. (2005) Structure, internal motions and association-dissociation kinetics of the i-motif dimer of d(5mCCTCACTCC). *Nucleic Acids Res.*, **33**, 5471–5481.
30. Nonin,S. and Leroy,J.L. (1996) Structure and conversion kinetics of a bi-stable DNA i-motif: broken symmetry in the [d(5mCCTCC)]4 tetramer. *J. Mol. Biol.*, **261**, 399–414.
31. Gallego,J., Chou,S.H. and Reid,B.R. (1997) Centromeric pyrimidine strands fold into an intercalated motif by forming a double hairpin with a novel T:G:G:T tetrad: solution structure of the d(TCCCGTTTCCA) dimer. *J. Mol. Biol.*, **273**, 840–856.
32. Nonin-Lecomte,S. and Leroy,J.L. (2001) Structure of a C-rich strand fragment of the human centromeric satellite III: a pH-dependent intercalation topology. *J. Mol. Biol.*, **309**, 491–506.
33. Han,X., Leroy,J.L. and Gueron,M. (1998) An intramolecular i-motif: the solution structure and base-pair opening kinetics of d(5mCCT3CCT3ACCT3CC). *J. Mol. Biol.*, **278**, 949–965.
34. Scheerhagen,M.A., Bokma,J.T., Vlaanderen,C.A., Blok,J. and van Grondelle,R. (1986) A specific model for the conformation of single-stranded polynucleotides in complex with the helix-destabilizing protein GP32 of bacteriophage T4. *Biopolymers*, **25**, 1419–1448.
35. Kypr,J., Kejnovska,I., Renciuk,D. and Vorlickova,M. (2009) Circular dichroism and conformational polymorphism of DNA. *Nucleic Acids Res.*, **37**, 1713–1725.
36. Mergny,J.L., Lacroix,L., Han,X.G., Leroy,J.L. and Helene,C. (1995) Intramolecular Folding of Pyrimidine Oligodeoxynucleotides into an I-DNA Motif. *J. Am. Chem. Soc.*, **117**, 8887–8898.
37. Li,T., Ackermann,D., Hall,A.M. and Famulok,M. (2012) Input-dependent induction of oligonucleotide structural motifs for performing molecular logic. *J. Am. Chem. Soc.*, **134**, 3508–3516.
38. Zhang,L., Guo,S., Zhu,J., Zhou,Z., Li,T., Li,J., Dong,S. and Wang,E. (2015) Engineering DNA three-way junction with multifunctional moieties: sensing platform for bioanalysis. *Anal. Chem.*, **87**, 11295–11300.
39. Seeman,N.C. (1982) Nucleic acid junctions and lattices. *J. Theor. Biol.*, **99**, 237–247.

40. Han,D., Pal,S., Yang,Y., Jiang,S., Nangreave,J., Liu,Y. and Yan,H. (2013) DNA gridiron nanostructures based on four-arm junctions. *Science*, **339**, 1412–1415.
41. Goodman,R.P., Schaap,I.A., Tardin,C.F., Erben,C.M., Berry,R.M., Schmidt,C.F. and Turberfield,A.J. (2005) Rapid chiral assembly of rigid DNA building blocks for molecular nanofabrication. *Science*, **310**, 1661–1665.
42. Erben,C.M., Goodman,R.P. and Turberfield,A.J. (2007) A self-assembled DNA bipyramid. *J. Am. Chem. Soc.*, **129**, 6992–6993.
43. Zuo,X., Xiao,Y. and Plaxco,K.W. (2009) High specificity, electrochemical sandwich assays based on single aptamer sequences and suitable for the direct detection of small-molecule targets in blood and other complex matrices. *J. Am. Chem. Soc.*, **131**, 6944–6945.
44. Liedl,T. and Simmel,F.C. (2005) Switching the conformation of a DNA molecule with a chemical oscillator. *Nano Lett.*, **5**, 1894–1898.
45. Shu,W., Liu,D., Watari,M., Riener,C.K., Strunz,T., Welland,M.E., Balasubramanian,S. and McKendry,R.A. (2005) DNA molecular motor driven micromechanical cantilever arrays. *J. Am. Chem. Soc.*, **127**, 17054–17060.
46. Liedl,T., Olapinski,M. and Simmel,F.C. (2006) A surface-bound DNA switch driven by a chemical oscillator. *Angew. Chem., Int. Ed.*, **45**, 5007–5010.
47. Liu,D., Bruckbauer,A., Abell,C., Balasubramanian,S., Kang,D.J., Klenerman,D. and Zhou,D. (2006) A reversible pH-driven DNA nanoswitch array. *J. Am. Chem. Soc.*, **128**, 2067–2071.
48. Liu,H.J., Xu,Y., Li,F.Y., Yang,Y., Wang,W.X., Song,Y.L. and Liu,D.S. (2007) Light-driven conformational switch of i-motif DNA. *Angew. Chem., Int. Ed.*, **46**, 2515–2517.
49. Cho,E.J., Yang,L., Levy,M. and Ellington,A.D. (2005) Using a deoxyribozyme ligase and rolling circle amplification to detect a non-nucleic acid analyte, ATP. *J. Am. Chem. Soc.*, **127**, 2022–2023.
50. Li,N. and Ho,C.M. (2008) Aptamer-based optical probes with separated molecular recognition and signal transduction modules. *J. Am. Chem. Soc.*, **130**, 2380–2381.